Electrocatalysis

DOI: 10.1002/anie.201203078

The Role of Co-Adsorbed CO and OH in the Electrooxidation of Formic Acid on Pt(111)**

*Wang Gao, Jonathan E. Mueller, Qing Jiang, and Timo Jacob**

The electrooxidation of formic acid (HCOOH) on platinum-group metals has been widely studied for its great relevance to electrochemistry as a prototype reaction for the electrooxidation of small organics and its importance in understanding low-temperature fuel cells.[1,2] It is generally accepted that electrooxidation of HCOOH on Pt proceeds by a dual-path mechanism consisting of indirect and direct paths.[1c] In the indirect path, HCOOH is converted into adsorbed CO and then to CO_2. In the direct path, HCOOH is converted into CO_2 via a reactive intermediate, whose identity is still disputed. Unfortunately, the intermediates from both the indirect and direct paths compete with each another for adsorption sites and the opportunity to react with oxidizers (e.g. OH) on the surface. This competition couples these reaction paths kinetically, hampering the elucidation of their individual reaction mechanisms.[3,4]

In situ infrared reflection-adsorption spectroscopy (IRAS) identifies adsorbed CO, resulting from HCOOH dehydration, as the key reaction intermediate in the indirect path. However, a build-up of CO is observed to poison the system.[1d,e] In contrast, the identity of the reactive intermediate along the direct path is still controversial. Wilhelm and coworkers initially suggested either COH or CHO.[1f] Others have long assumed it to be COOH.[1c,h,2c] Using IR spectroscopy, Osawa et al. and Feliu et al. found that formate (HCOO) is the reactive intermediate and that the oxidation of HCOO to CO_2 is the rate-determining step for formic acid oxidation.[3–8] In contrast, Behm et al. argue that weakly adsorbed HCOOH might be the key intermediate, leaving HCOO as a spectator.[9–11] The electrochemical and spectral data obtained under both static and flow conditions, which provide the basis for these proposed reactive intermediates, are essentially identical. However, different interpretations of the non-linear relationship between the measured current and the formate coverage lead to different conclusions.[4]

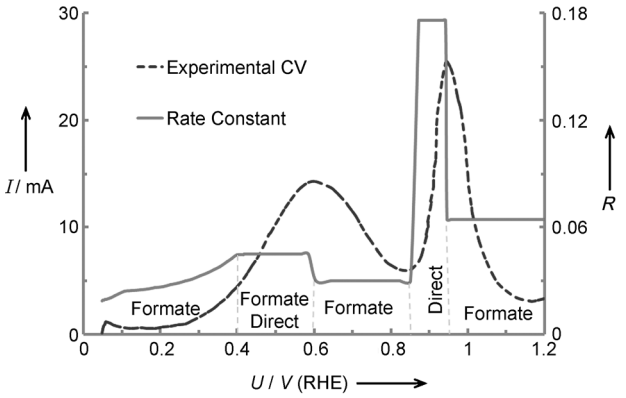

Figure 1. The potential-dependent rate constants (R) and the experimental CV.[5] The potential sweep rate is 50 $mV s^{-1}$.

Cyclic voltammograms (CVs) of HCOOH oxidation (Figure 1) show that the current (I) first peaks around 0.6 V as the potential (U) increases. The current then remains stable or decreases between 0.6 and 0.8 V in what is termed the negative differential resistance (NDR) region. A sharp, increasing around 0.95 V follows the NDR region.[3,5,10,12–14] During this process, IR spectroscopy measurements reveal that the polycrystalline Pt surface has a relatively constant coverage of CO below 0.8 V. Above 0.8 V, the coverage of adsorbed CO rapidly decreases due to oxidation, while HCOO quickly increases with increasing potential, until the surface is nearly saturated with HCOO at above 0.9 V. Once the CO coverage is almost completely depleted (ca. 0.95 V), the coverage of HCOO rapidly decreases with increasing potential up to 1.2 V.

Thus, these IR measurements suggest that the CV curve can be understood in terms of CO adsorption, desorption, and oxidation by OH. Nevertheless, the detailed roles of adsorbed CO and OH have yet to be elucidated, substantially hindering our understanding of the mechanism of this fundamental reaction.

First principles simulations have already been useful in studying HCOOH oxidation. Two density functional theory (DFT) studies indicate that HCOOH oxidation under electrochemical conditions either proceeds via intermediate COOH or initiates from a weakly adsorbed configuration of HCOOH, in which the C–H bond is in a "down" configuration.[15] However, several independent theoretical investigations report that the HCOOH adsorption models used in these studies do not correspond to the most energetically favorable structure.[16,17] More recently, using a gas phase model (i.e. without treating solvation effects), we found that bidentate formate ($HCOO_B$*) is the reactive intermediate in HCOOH oxidation. This result is fully consistent with

[*] Dr. W. Gao, Dr. J. E. Mueller, Prof. Dr. T. Jacob
Institut für Elektrochemie, Universität Ulm
89069 Ulm (Germany)
E-mail: timo.jacob@uni-ulm.de
Prof. Dr. Q. Jiang
School of Materials Science and Engineering, Jilin University
130022 Changchun (China)

[**] We gratefully acknowledge support by the "Deutsche Forschungsgemeinschaft" (DFG) within the Emmy-Noether-Program and the Forschergruppe FOR-1376 as well as by the bw-grid for computing resources.

Supporting information (Experimental Section) for this article is available on the WWW under http://dx.doi.org/10.1002/anie.201203078.

experimental studies under ultra-high vacuum (UHV) conditions.[17a,18] We also investigated the same process in the presence of solvent and under the influence of an electrode potential to mimic electrochemical conditions. We found that the direct path consists of a dual-pathway mechanism, which includes a formate pathway involving the $HCOO_B$ intermediate [Eq. (1)], and a direct pathway, involving a highly transient CO_2 intermediate [Eq. (2)].[17b]

$$HCOOH^* \rightarrow HCOO^* + H^+ + e^- \rightarrow CO_2 + H^+ + e^- \quad (1)$$

$$HCOOH^* \rightarrow COO^* + 2H^+ + 2e^- \rightarrow CO_2 \quad (2)$$

Based on these studies, we aim to elucidate the role of co-adsorbed CO and OH on the overall reaction mechanism and thus establish the identity of the disputed intermediate(s).

In our previous study,[17b] in which we compared various explicit solvation models, we found that Model B (Figure 2; the nomenclature refers to Ref. [17b]), in which HCOOH is fully embedded in a water bilayer network, provided the most reliable model. To investigate the role of surface CO and OH in HCOOH oxidation, fractional coverages of CO (Model C), OH (Model D), or combinations of both (Model F) were co-adsorbed with solvated HCOOH. The presence of the indirect pathway has already been established through the experimental identification of CO; we now consider the direct and formate pathways, because they are believed to dominate the kinetics of the oxidation process. Various reaction steps can be proposed for these two pathways depending on the surface coverages of CO and OH. By considering the energetics of these different pathways in the presence of an applied electrode potential, our results reveal the detailed roles played by CO and OH in HCOOH oxidation and clarify the mechanism for this fundamental electrocatalytic process.

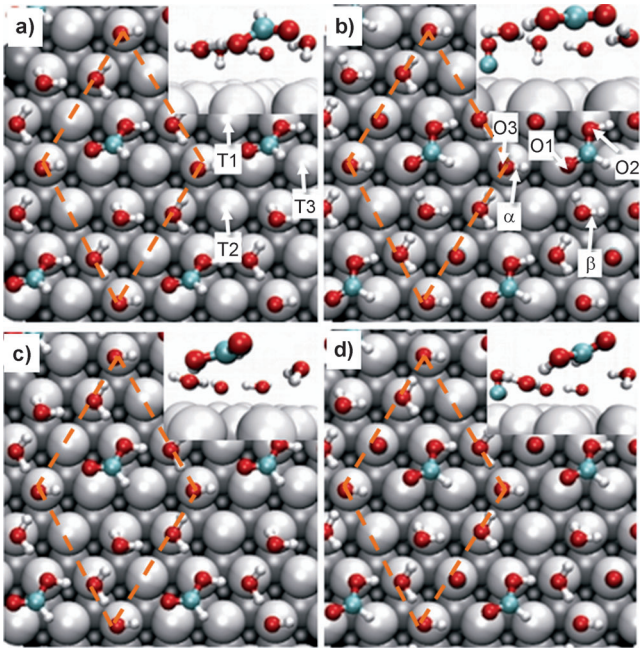

Figure 2. a) Solvation Model B having HCOOH structures with four water molecules per unit cell on Pt(111). b)–d) Models C_1, D_1, and F_1 which have 1/9 ML co-adsorbed CO, 1/9 ML co-adsorbed OH, and both of 1/9 ML co-adsorbed CO and 1/9 ML co-adsorbed OH, respectively. Insets present side views of the interface. T1, T2, T3 in (a) are the different top sites; O1, O2, O3 in (b) are the different O atoms; α and β in (b) denote the different position of water. (More models in higher coverage of CO and OH are shown in Supporting Information.)

Experimental measurements of CO* on Pt(111) in the presence of HCOOH* reveal two adsorption geometries: bridge-bonded CO* (CO_B), and top-bonded (or linearly bonded) CO* (CO_L). The surface coverage of CO_B is low and nearly independent of the applied potential, while the coverage of CO_L depends strongly on the applied current.[5] Consequently, herein, we neglect CO_B and focus on the potential-dependent effects of co-adsorbed CO_L.

Table 1 shows the energies for HCOOH oxidation pathways investigated using Models B–F (detailed mechanisms are in the Supporting Information). The preferred structure for the addition of 1/9 monolayer (ML) CO* is shown in Figure 1b (Model C_1). In this case, the formate pathway clearly dominates at low potentials, with a barrier of $E_a = 1.19$ eV at $U = 0$ V, which involves a coupled proton–electron-transfer (CPET) process as the rate-determining step. As the potential increases, the decomposition of monodentate formate ($HCOO_M$*) to CO_2 ($E_a = 0.93$ eV) in the formate pathway, and the decomposition of HCOOH* to CO_2* ($E_a = 0.91$ eV) in the direct pathway, become increasingly important. This behavior is consistent with that of Model B, indicating that the presence of up to 1/9 ML of CO* does not substantially alter the HCOOH oxidation mechanism. Nevertheless, the increase of the reaction barriers in the presence of 1/9 ML of CO*, reveals that CO* suppresses HCOOH oxidation, as an experimental study has already revealed.[3]

The presence of additional CO*, up to 2/9 ML as in Model C_2 (see Figure S1c in the Supporting Information), does not significantly alter either the structure of the $HCOOH/H_2O$ network (Table S2) or the HCOOH oxidation mechanism. Consequently, the barriers for the individual reaction processes in Model C_2 are only slightly higher than the barriers for the corresponding processes in Model C_1 (Table 1). Thus, low coverages of CO* (1/9–2/9 ML) suppress HCOOH oxidation by increasing the reaction barriers, without substantially altering the basic mechanistic steps.[3] Nevertheless, we expect that further increasing the coverage of CO* would eventually block the active sites for HCOOH oxidation, resulting in more drastic changes.

Table 1: The highest barriers of the minimum energy pathways for HCOOH oxidation at different potentials. Energy barriers in eV.

Model	Formate pathway		Direct pathway	
	$U = 0$ V	$U > 0.3$ V	$U = 0$ V	$U > 0.3$ V
B	1.02	0.73	1.31	0.79
C_1	1.19	0.93	1.69	0.91
C_2	1.10	0.97	1.77	0.99
D_1	–	0.81	–	–
D_2	–	–	–	0.79
D_3	–	0.71	–	0.77
F_1	–	–	–	0.50
F_2	–	–	–	0.59
F_3	–	–	–	0.45
F_4	–	–	–	0.59

Models D_1–D_3 are obtained by removing H from either one or both of the two most acidic water molecules in Model B. Models D_1 and D_2 (Figure 1c; Figure S1e) each contain one OH molecule per unit cell and have similar energies. However, model D_1 favors the formate pathway ($E_a = 0.81$ eV), while model D_2 favors the direct pathway ($E_a = 0.79$ eV). Thus, at low coverages of OH* we expect HCOOH oxidation to proceed via a dual-path mechanism, involving both pathways depending on the local position of OH*. Moreover, the step with the highest barrier is no longer associated with a CPET process, but rather with either the cleavage of a $HCOO_B$* surface bond to form $HCOO_M$*, or the decomposition of HCOOH* to CO_2*. In contrast to the mechanism observed with Model B (no co-adsorbed CO* and OH*), the steps with the highest barriers now are of pure chemical nature (i.e. are independent of the applied potential). This difference in behavior is primarily due to OH* avoiding a potential-dependent CPET step in the HCOOH oxidation process. Thus, OH* not only takes the place of water in the hydrogen-bond network, but also acts as a reducing agent in the oxidation of HCOOH.

When we oxidize both waters to form OH* (Model D_3, $\theta_{OH} = 2/9$ ML), we find that the steps with the highest barriers for each pathway are potential independent and have similar values ($E_a = 0.71$ and 0.77 eV for the formate and direct pathways, respectively). The small difference between these barriers suggests that HCOOH oxidation proceeds via a dual-path mechanism in this case as well.

Surface OH* is only stable for electrode potentials above 0.5 V.[19] In this potential range the highest barriers in the minimum energy pathway without OH* ($E_a = 0.73$ and 0.79 eV for Model B) are similar to the barriers with OH* (Models D). Thus, OH* only has a minor effect on the reactivity of HCOOH oxidation. Nevertheless, its presence breaks the rate constant's dependence on the applied potential.

The oxidation of HCOOH under the simultaneous influence of co-adsorbed CO* and OH* is modeled by adding CO* to Models D_1–D_3 to produce Models F_1–F_4 (Figure 1d; Figures S1h–j). For $U > 0.5$ V and low surface coverages of CO* and OH* (1/9 ML for each in Models F_1 and F_2) the direct pathway dominates. Desorption of CO_2 ($E_a = 0.50$ eV) is the step with the highest barrier in the case of Model F_1, while the double dehydrogenation of formic acid HCOOH* to CO_2* ($E_a = 0.59$ eV) has the highest barrier in the case of Model F_2. As neither of these processes involves a CPET, the barriers for these processes are independent of the applied potential. They are up to 0.29 eV lower in energy than in the absence of CO* and OH* ($E_a = 0.79$ eV, Model B). Thus, together OH* and CO* promote the direct pathway, while suppressing the formate pathway by increasing its barriers by up to 0.23 eV (0.96 eV and 0.74 eV for Models F_1 and F_2, respectively, compared to 0.73 eV for Model B).

Next, we consider the presence of additional OH* by deprotonating an additional water in Model F_1 to construct Model F_3, which contains 2/9 ML OH* and 1/9 ML CO*. This additional OH* does not change the overall mechanism of HCOOH oxidation, but reduces the direct pathway barrier to 0.45 eV, further promoting the reaction.

Finally, we model the effects of additional CO* by adding CO* to Model F_1 to form Model F_4, which contains 2/9 ML CO* and 1/9 ML OH*. While the additional CO* increases the barrier for the direct pathway by 0.09 eV, it is still preferred over the formate pathway by 0.48 eV. Thus, increasing the coverage of CO* beyond 1/9 ML, in the presence of co-adsorbed OH*, adversely affects HCOOH oxidation.

The presence of either CO* or OH* alone is able to promote the activity of Pt(111) for HCOOH oxidation; however, surprisingly, the combination of CO* and OH* is. We attribute this synergy to a combination of changes in the hydrogen-bond network and the induction of a surface charge. Based on hydrogen-bond lengths involving HCOOH (Table S2), we estimate that the hydrogen bonds in Models C_1 and D_2 are 0.16 eV and 0.27 eV, respectively, stronger than in Model B. In contrast, the hydrogen bonding in Model F_1 is 0.13 eV weaker. Because these hydrogen bonds must be broken to form the product, increasing their strength suppresses HCOOH oxidation, while weakening them promotes it.

We find that OH* induces a positive charge that distributes itself across the entire Pt surface (Models D_2 and F_1 in Figures S5c,d), while the positive charge induced by CO* is localized directly below it (Model C_1 in Figure *S*5b). Just as Hartnig et al. find that a positive Pt surface charge activates HCOOH oxidation by lowering the critical C–H activation barrier,[16b] we suspect that the delocalized surface charge induced by OH* in our system does the same. These changes in the hydrogen-bond network and surface charge interact in such a way that in isolation CO* (Model C_1) and OH* (Model D_2) suppress or have little effect on HCOOH oxidation. However, the presence of both CO* and OH* (Model F_1) substantially promotes it. (For mechanistic details see Supporting Information.)

Comparing our results with experimental studies requires an appropriate choice of surface model to match the experimental surface coverage conditions. Thus, we must determine the relevant surface coverages of CO (θ_{CO}) and OH (θ_{OH}) on Pt(111) for electrode potentials of interest. Based on IR spectroscopy studies, Osawa et al. estimate that below $U = 0.85$ V, θ_{COL} is in the range of 0.1–0.3 ML, and it decreases until it nearly reaches zero at $U = 0.95$ V.[6] Thus, we assume $\theta_{COL} = 2/9$ ML for the approximately constant coverage region[5] for $U < 0.85$ V, $\theta_{COL} = 0$ for $U > 0.95$ V,[3] and $\theta_{COL} = 1/9$ ML for the region between. Regarding OH*, experiments first detect OH* at $U = 0.5$ V; however, its coverage is still very low at $U = 0.6$ V.[19] By $U = 0.85$ V, we assume the OH coverage has increased to $\theta_{OH} = 2/9$ ML. Thus, for $0 < U < 0.6$ V, we utilize Model C_2 ($\theta_{CO} = 2/9$ ML, $\theta_{OH} = 0$). We anticipate that a more complex model will be necessary to account for the water dissociation that takes place in the NDR region ($0.6 < U < 0.85$ V), and thus approximate this region by only considering the coupling between COOH and HCOOH. For $0.85 < U < 0.95$ V, Model F_3 ($\theta_{CO} = 1/9$ ML, $\theta_{OH} = 2/9$ ML) seems to be appropriate. Finally, for $0.95\text{ V} < U < 1.2$ V, we utilize Model D_3 ($\theta_{CO} = 0$, $\theta_{OH} = 2/9$ ML), which ignores the possibility of surface oxidation. Thus, we obtain a potential-dependent

picture of the preferred reaction mechanism (Scheme 1), leading to the overall rate constant (R) for the HCOOH oxidation process as a function of U (Figure 1).

Starting from $U = 0$ V, R increases as the potential increases to 0.4 V, at which point it reaches a plateau that lasts at least to the beginning of the NDR region ($U = 0.6$ V). On the other side of the NDR region ($U > 0.85$ V), it achieves its maximum value before entering the final region we consider begins at $U = 0.95$ V, where we find a lower rate that lasts until at least $U = 1.2$ V. These trends are compatible with the experimental CV curve obtained over $0 < U < 1.2$ V (Figure 1).

The initial oxidation, beginning at $U = 0$ V, is dominated by the formate mechanism, which has the rate-limiting step associated with the potential-dependent CPET process. Because the $HCOO_B$ immediately precedes the rate-limiting CPET process, we expect $HCOO_B$ to be detected at these low potentials. Experiments fulfill these expectations, finding that formate appears around $U = 0.2$ V in the spectra.[4,10] As the potential approaches $U = 0.4$ V, the direct pathway becomes competitive with the formate pathway. We expect this to result in an overall dual-path mechanism, which continues at least to the beginning of the NDR region ($U = 0.6$ V). However, the high coverage of CO and bridge-bonded formate, present in experiments, but not included in our model, may deactivate the direct pathway in favor of the formate pathway.

Beginning in the NDR region, OH plays an increasingly important role. Here it easily reacts with CO to form COOH, which forms a hydrogen bond to the carbonyl oxygen of HCOOH, as part of a distorted COOH–HCOOH–H_2O network. The high coverage of CO ties up the surface OH, making it unavailable for HCOOH oxidation. More importantly, the distorted network increases the barrier for the direct pathway HCOOH→CO_2* from 0.99 eV (as in Model C_2 at $U = 0.4 \approx 0.6$ V) to 1.50 eV, while having virtually no effect on the barrier for the formate pathway. Thus, by disabling the direct pathway, the presence of distorted COOH above 0.60 V may partially explain the decreasing current in the NDR region. Contributions from the adsorption of other (still unknown) poisoning species may also play an important role.[5,7]

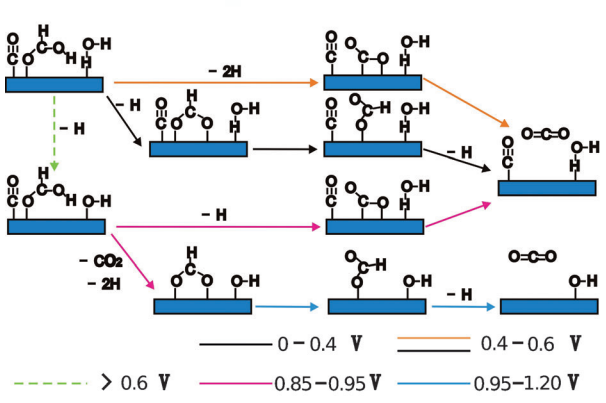

Scheme 1. Preferred reaction pathway for different electrode potential regimes.

Moving beyond the NDR region, for $0.85 \text{ V} < U < 0.95$ V HCOOH is oxidized almost exclusively through the direct pathway ($E_a = 0.45$ eV). We find that the co-effect of CO* and OH* here effectively promotes HCOOH oxidation, challenging the traditional conception of CO* always acting as a poison in HCOOH oxidation. Unfortunately, the oxidative removal of this promoting CO* at higher potentials limits this efficient mechanism to a relatively narrow potential range. During this process, the formation of $HCOO_B$* (the first step in the formate pathway) is nearly barrierless ($E_a \approx 0$ eV). However, because the subsequent decomposition of $HCOO_M$* to form CO_2 has a high barrier ($E_a = 0.80$ eV), we expect HCOO* to rapidly accumulate on the surface. Indeed, experiments observe this accumulation beginning at $U \approx 0.85$ V and peaking around $U \approx 0.95$ V. We expect this excess HCOO* to suppress HCOOH oxidation by blocking surface sites, which would otherwise be available for the adsorption and oxidation of additional HCOOH through the direct pathway.

However, beyond 0.95 V, HCOO decomposes to CO_2 under the influence of OH* with a barrier of $E_a = 0.71$ eV, rapidly reducing the formate coverage as observed in experiments.[3,5] The experimentally observed decay of current for potentials above $U = 0.95$ V is usually ascribed to the oxidation of the Pt surface.[3] If we assume that the surface oxide (which we have not modeled herein) is a poor catalyst, then we might expect the decrease in reactivity to mirror the growth of surface oxide, as the formate-pathway-catalyzing pure Pt surface gives way to less-active Pt oxide. Thus, because the surface is not oxidized instantaneously, we expect the formate pathway to remain active through the initial stages of surface-oxide formation. While thermodynamically the formation of an oxide should form for $E > 1.2$ eV,[19] the kinetics are limited by the energy barrier associated with oxygen incorporation, which varies with the coordination of the local surface sites. Thus, qualitatively faster oxide formation at defects or step-edges might be expect compared to terrace sites.

The influence of the potential sweep rate exerts a significant influence on the CV curve. In particular, if the rates were decreased, the oxidation peak at 0.95 V in Figure 1 would shift toward the left and eventually merge with the peak at 0.6 V to yield a single peak for a stationary-state system.[3,20] It has also been found that the Pt surface is severely poisoned by CO for very low rates (3 $mV s^{-1}$). Thus the CV at 50 $mV s^{-1}$ is the optimal experimental setup for us to make comparisons with, because it avoids CO poisoning while allowing for (quasi-stationary state) HCOOH oxidation.

The deposition of a monolayer of CO* on the Pt electrode prior to the oxidation of HCOOH, results in the total suppression of the first current peak in the CV, and a positive shift of the second current peak ($\Delta U \approx 0.1$ V), coinciding with a shift in the growth of the HCOO coverage.[3] The total suppression of the first current peak is easily explained by the inaccessibility of surface active sites for HCOOH oxidation because of the high coverage of CO*. Furthermore, the oxidative removal of CO* requires OH*, which is also required for HCOOH oxidation. Thus the competition with excess CO* for surface sites and OH* molecules decreases the

rate of HCOOH oxidation, as both the build-up of OH* and the decomposition of CO*, to reach the optimal coverages required to synergistically promote HCOOH oxidation, as our model predicts, are delayed, resulting in a positive shift in the second peak. The delayed growth of the HCOO coverage, observed in experiments, is also consistent with this interpretation.

A typical chronoamperogram reveals that when the electrode potential is stepped up from 0.05 V to 0.9 V, CO* is completely oxidized within seconds.[4] Within this short time, the current (I) quickly decays following an initial spike and the HCOO coverage drastically increases. The behavior of I corresponds to the rapid oxidation and disappearance of CO*. Thus, Model F_3 (1/9 ML of CO* and 2/9 ML of OH*) is initially relevant, followed by Model D_3 (0 ML of CO* and 2/9 ML of OH*) once CO* has been oxidized away. The low barrier ($E_a \approx 0$) to form HCOO* coupled with the high barrier ($E_a = 0.80$) to convert it into product results in the initial build-up of HCOO*. We anticipate that the formation of surface oxide (experimentally identified as Pt_4OH near 0.9 V, but not included in our current model) hinders the rate of formic acid oxidation.[19]

Stepping U to 0.6 V (following the few seconds at 0.9 V) results in an immediate increase in I then a gradual decrease as the HCOO coverage drops by a fraction of its initial value and quickly converges to a new constant. Under the reduced potential we anticipate that the Pt oxide is quickly reduced, returning the metal surface to its initial state. This frees up additional surface sites for HCOOH oxidation, resulting in an increased oxidation rate, which slightly reduces the concentration of HCOO. Because the surface is initially covered with HCOO, this must first decompose under surface conditions best represented by Model D_3 ($E_a = 0.71$ eV). As HCOO is oxidized, surface sites become available for the adsorption of HCOOH. The condition of the surface is probably now best represented by a combination of Models B, D_1, or D_1 ($E_a =$ 0.73, 0.79, or 0.81 eV), which all have a higher reaction barrier than Model D_3 ($E_a = 0.71$ eV). Thus, the removal of OH* from the surface results in a slower HCOOH oxidation rate, corresponding to the gradual decrease in I observed.

In conclusion, we find that CO* (in the absence of OH*) adversely affects HCOOH oxidation: not only by blocking active sites, but also by retarding the rates of important reaction steps. On the other hand, OH* (in the absence of CO*) does not significantly alter the reactivity of HCOOH oxidation on a clean Pt surface. However, at high potentials it oxidizes the Pt surface, and thus poisons the reaction by blocking active sites. Nevertheless, we find that CO* and OH* have a synergistic co-effect, such that relatively low coverages of both effectively promote HCOOH oxidation. These solitary and synergistic behaviors of CO* and OH* successfully explain the CV measurements of the electrooxidation of HCOOH in the potential range of 0.0–1.2 V. Further studies on the complete role of CO* and OH* will focus on the oxidation of the Pt surface.

Received: April 21, 2012
Revised: July 7, 2012
Published online: August 21, 2012

Keywords: density functional theory · electrochemistry · formic acid · heterogeneous catalysis · platinum

[1] a) M. W. Breiter, *J. Electroanal. Chem.* **1967**, *14*, 407 – 413; b) A. Capon, R. Parson, *J. Electroanal. Chem.* **1973**, *44*, 1 – 7; c) A. Capon, R. Parsons, *J. Electroanal. Chem.* **1973**, *45*, 205 – 231; d) K. Kunimatsu, H. Kita, *J. Electroanal. Chem.* **1987**, *218*, 155 – 172; e) D. S. Corrigan, M. J. Weaver, *J. Electroanal. Chem.* **1988**, *241*, 143 – 162; f) S. Wilhelm, W. Vielstich, H. Buschmann, T. Iwasita, *J. Electroanal. Chem.* **1987**, *229*, 377 – 384; g) R. Parsons, T. VanderNoot, *J. Electroanal. Chem.* **1988**, *257*, 9 – 45; h) C. Lamy, J. M. Leger, *J. Chim. Phys. Phys.-Chim. Biol.* **1991**, *88*, 1649 – 1671; i) N. Kizhakevariam, M. J. Weaver, *Surf. Sci.* **1994**, *310*, 183 – 197.

[2] a) B. Beden, J. M. Leger, C. Lamy in *Modern Aspects of Electrochemistry*, *Vol. 22* (Eds.: J. O. M. Bockris, B. E. Conway, R. E. White), Plenum, New York, **1992**, p. 97; b) T. D. Jarvi, E. M. Stuve in *Electrocatalysis* (Eds.: J. Lipkowski, P. Ross), Wiley-VCH, **1998**, pp. 75 – 153; c) S.-G. Sun in *Electrocatalysis* (Eds.: J. Lipkowski, P. N. Ross), Wiley-VCH, New York, **1998**, p. 243.

[3] G. Samjeské, A. Miki, S. Ye, M. Osawa, *J. Phys. Chem. B* **2006**, *110*, 16559 – 16566.

[4] M. Osawa, K. Komatsu, G. Samjeské, T. Uchida, T. Ikeshoji, A. Cuesta, C. Gutiérrez, *Angew. Chem.* **2011**, *123*, 1191 – 1195; *Angew. Chem. Int. Ed.* **2011**, *50*, 1159 – 1163.

[5] G. Samjeské, M. Osawa, *Angew. Chem.* **2005**, *117*, 5840 – 5844; *Angew. Chem. Int. Ed.* **2005**, *44*, 5694 – 5698.

[6] G. Samjeské, A. Miki, S. Ye, A. Yamakata, Y. Mukouyama, H. Okamoto, M. Osawa, *J. Phys. Chem. B* **2005**, *109*, 23509 – 23516.

[7] Y. Mukouyama, M. Kikuchi, G. Samjeské, M. Osawa, H. Okamoto, *J. Phys. Chem. B* **2006**, *110*, 11912 – 11917.

[8] V. Grozovski, F. J. Vidal-lglesias, E. Herrero, J. M. Feliu, *ChemPhysChem* **2011**, *12*, 1641 – 1644.

[9] Y. X. Chen, M. Heinen, Z. Jusys, R. J. Behm, *Angew. Chem.* **2006**, *118*, 995 – 1000; *Angew. Chem. Int. Ed.* **2006**, *45*, 981 – 985.

[10] Y. X. Chen, M. Heinen, Z. Jusys, R. J. Behm, *Langmuir* **2006**, *22*, 10399 – 10408.

[11] Y. X. Chen, M. Heinen, Z. Jusys, R. J. Behm, *ChemPhysChem* **2007**, *8*, 380 – 385.

[12] P. Strasser, M. Lübke, F. Raspel, M. Eiswirth, G. Ertl, *J. Chem. Phys.* **1997**, *107*, 979 – 990.

[13] G. Lu, A. Crown, A. Wieckowski, *J. Phys. Chem. B* **1999**, *103*, 9700 – 9711.

[14] H. Okamoto, W. Kon, Y. Mukouyama, *J. Phys. Chem. B* **2005**, *109*, 15659 – 15666.

[15] a) M. Neurock, M. Janik, A. Wieckowski, *Faraday Discuss.* **2009**, *140*, 363 – 378; b) H. Wang, Z. Liu, *J. Phys. Chem. C* **2009**, *113*, 17502 – 17508.

[16] a) I. Bakó, G. Pálinkás, *Surf. Sci.* **2006**, *600*, 3809 – 3814; b) C. Hartnig, J. Grimminger, E, Spohr, *J. Electroanal. Chem.* **2007**, *607*, 133 – 139.

[17] a) W. Gao, J. A. Keith, J. Anton, T. Jacob, *Dalton Trans.* **2010**, *39*, 8450 – 8456; b) W. Gao, J. A. Keith, J. Anton, T. Jacob, *J. Am. Chem. Soc.* **2010**, *132*, 18377 – 18385.

[18] a) M. R. Columbia, P. A. Thiel, *Surf. Sci.* **1990**, *235*, 53 – 59; b) M. R. Columbia, A. M. Crabtree, P. A. Thiel, *J. Am. Chem. Soc.* **1992**, *114*, 8450 – 8456.

[19] H. Angerstein-Kozlowska, B. E. Conway, W. B. A. Sharp, *J. Electroanal. Chem.* **1973**, *43*, 9 – 36.

[20] H. Okamoto, W. Kon, Y. Mukouyama, *J. Phys. Chem. B* **2004**, *108*, 4432 – 4438.

